Etching-Free Epitaxial Growth of Gold on Silver Nanostructures for High Chemical Stability and Plasmonic Activity

Hongpo Liu, Tingzhuo Liu, Lei Zhang, Lu Han, Chuanbo Gao, and Yadong Yin**

A robust method for epitaxial deposition of Au onto the surface of Ag nanostructures is demonstrated, which allows effective conversion of Ag nanostructures of various morphologies into Ag@Au counterparts, with the anisotropic ones showing excellent plasmonic properties comparable to the original Ag nanostructures while significantly enhanced stability. Sulfite plays a determining role in the success of this epitaxial deposition as it strongly complexes with gold cations to completely prevent galvanic replacement while it also remains benign to the Ag surface to avoid any ligand-assisted oxidative etching. By using Ag nanoplates as an example, it is shown that the corresponding Ag@Au nanoplates possess remarkable plasmonic properties that are virtually Ag-like, in clear contrast to Ag@Au nanospheres that exhibit much lower plasmonic activities than their Ag counterparts. As a result, they display high durability and activities in surface-enhanced Raman scattering applications. This strategy may represent a general platform for depositing a noble metal on less stable metal nanostructures, thus opening up new opportunities in rational design of functional metal nanomaterials for a broad range of applications.

1. Introduction

Coinage metal (Au, Ag, Cu) nanoparticles show unique optical properties owing to their strong localized surface plasmon resonance (LSPR) in the visible range of light,[1] which has enabled their broad use in applications including surface-enhanced Raman spectroscopy (SERS)[2] and fluorescence,[3] biosensing,[4] imaging,[5] therapeutics,[6] and catalysis.[7] In particular, Au nanospheres have received intensive attention owing to their convenient synthesis and functionalization, excellent stability, and biocompatibility.[8] However, they display much weaker LSPR compared with Ag nanospheres, which limits their performance in many plasmon-based applications. Theoretically, the weak LSPR of the Au nanospheres can be attributed to the coupling of the LSPR excitations with the *d*–*sp* interband electron transitions extending to the visible range of the spectrum (≈520 nm).[9] It is therefore hypothesized that anisotropic Au nanocrystals are able to compare favorably with their Ag counterparts in producing remarkable LSPR that shifts away from the region of the interband transitions to long wavelengths of the spectrum. However, other than Au nanorods that were discovered more than a decade ago,[10] there have been rare reports on the high-yield synthesis of high-quality anisotropic nanocrystals of Au such as nanoplates with tightly controllable structural and optical properties,[11] albeit their great significance to many biological applications due to the possibility of shifting their resonance wavelengths to near-infrared region where light absorption by tissue, blood, and water is minimal.[12]

In contrast to the difficulty in the synthesis of anisotropic Au nanocrystals, the last decade witnessed a great blossom in the development of Ag nanocrystals with a variety of morphologies, due to convenient availability of various mechanisms for effective guidance of their growth.[1a,13] For example, Ag nanoplates of uniform shape and tunable size can be reproducibly synthesized in high yield by photochemical, thermal, and seeded growth methods.[14] These Ag nanocrystals are promising templates for the epitaxial growth of Au to form a family of Ag@Au core/shell nanocrystals that are equivalent to pure Au nanocrystals in both surface and plasmonic property. However, galvanic replacement between Ag nanocrystals and the Au precursor, $HAuCl_4$, becomes the major challenge, which usually gives rise to hollow Au/Ag alloy nanostructures.[15] Seminal efforts have been made toward solving this problem including control of the reaction kinetics and thermodynamics. Examples of the former include tuning the pH and the addition rate of

H. Liu, T. Liu, L. Zhang, Prof. C. Gao
Center for Materials Chemistry
Frontier Institute of Science and Technology
Xi'an Jiaotong University
Xi'an, Shaanxi 710054, P.R. China
E-mail: gaochuanbo@mail.xjtu.edu.cn
H. Liu, T. Liu, L. Zhang, Prof. C. Gao
State Key Laboratory for Mechanical Behavior of Materials
Xi'an Jiaotong University
Xi'an, Shaanxi 710054, P.R. China
Prof. L. Han
School of Chemistry and Chemical Engineering
Shanghai Jiao Tong University
Shanghai 200240, P.R. China
Prof. Y. Yin
Department of Chemistry
University of California
Riverside, CA 92521, USA
E-mail: yadong.yin@ucr.edu

DOI: 10.1002/adfm.201502366

the Au precursor,[16] while the latter is typically represented by decreasing the reduction potential of the Au salt through coordinating to a strong ligand.[4,17] However, these efforts enabled deposition of only atomic layers of Au on Ag nanocrystals—whether the continuous overgrowth can be achieved is questionable due to the difficulty in avoiding further etching of the Ag nanocrystals, especially for thin plates which are highly reactive (Figure S1, Supporting Information). Although these nanocrystals could stay stable under mild conditions, they are unlikely to survive in many harsh conditions such as strongly oxidative environments in many practical applications.

In this work, we report our effort toward the synthesis of anisotropic Ag@Au core/shell nanoplates in high yield by epitaxial growth of a thick layer of Au on conventionally available Ag nanoplates and reveal their high stability and virtually Ag-like plasmonic properties. The key of our synthesis was to choose sulfite as an appropriate ligand, which strongly coordinates to Au cations but not to Ag cations in the mild reductive environment, so that both galvanic replacement and ligand-assisted oxidative etching to the Ag nanoplates can be reliably avoided. The experimental success enabled direct verification of the Ag-like plasmonic properties of the Ag@Au core/shell nanoplates by UV–vis spectroscopy, which was in good agreement with our theoretical simulations by finite element method (FEM).[18] The Ag@Au core/shell nanoplates thus displayed superior activity in SERS detection of molecules of interest in many harsh conditions. We believe this synthesis method is not limited to the conversion of various Ag nanostructures into Ag@Au core/shell ones but also represents a general platform for depositing a noble metal on less-stable metal nanostructures, thus opening up new avenues to functional metal nanomaterials for a broad range of applications.

2. Results and Discussion

2.1. Theoretical Investigation of the Plasmonic Properties of the Ag@Au Core/Shell Nanocrystals

In this study, we reasoned that Ag@Au core/shell nanocrystals with a Ag core and a thick Au shell are plasmonic property equivalents of their Au counterparts, and that the high anisotropy is critical for the nanocrystals to afford Ag-like plasmonic properties owing to the shifted LSPR bands from the region of the interband transitions to long wavelengths of the spectrum. To evaluate the plasmonic properties of the Ag@Au core/shell nanocrystals especially the superior plasmonic properties of the nanoplates, FEM has been employed to simulate the extinction efficiency and local electric field distribution of the nanocrystals from the theoretical perspective (**Figure 1**).

The results (Figure 1b,d) first confirmed that the plasmonic properties of the Ag@Au core/shell nanoplates are equivalent to those of the pure Au nanoplates, because both the extinction efficiency and the local electric field enhancement of the nanocrystals were very close. The Ag@Au core/shell nanoplates showed a redshift of the LSPR band relative to that of the pure Au ones due to the different dielectric core materials, which indicated that the Ag core can affect the overall plasmonic

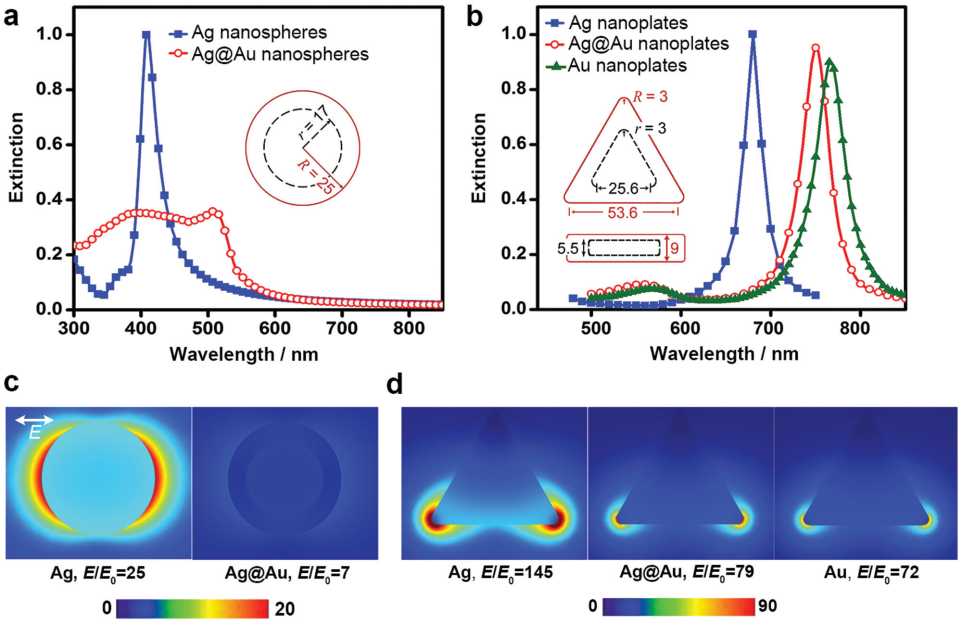

Figure 1. Plasmonic properties of the Ag@Au core/shell nanostructures simulated by FEM. a) LSPR extinction profile of the Ag@Au nanospheres in comparison with that of the Ag nanospheres. b) LSPR extinction profile of the Ag@Au nanoplates in comparison with those of the Ag and Au nanoplates. The overall size of the Ag, Au, and Ag@Au nanocrystals was the same in each comparison, while the thickness of the Au shell was fixed to be 8 nm for all the Ag@Au core/shell nanostructures. Insets schematically illustrate the geometrical models of the Ag@Au core/shell nanostructures; length unit: nm. c) Distributions of the electric field intensity in the proximity of the Ag and the Ag@Au nanospheres irradiated at their respective resonance wavelengths. d) Distributions of the electric field intensity in the proximity of the Ag, Ag@Au, and Au nanoplates irradiated at their respective resonance wavelengths.

properties to a minor extent. Therefore, the Ag@Au core/shell nanoplates are plasmonic property equivalents of pure Au nanoplates when a thick shell of Au is grown on their surfaces.

In the investigation of the anisotropy-dependent plasmonic properties of the Ag@Au core/shell nanocrystals, Ag nanospheres were chosen as typical plasmonic nanoparticles of an isotropic shape, which displayed a strong LSPR band at 410 nm of the wavelength (Figure 1a). However, the corresponding Ag@Au core/shell ones showed an LSPR band with greatly damped intensity at 510 nm of the wavelength. In addition, the Ag@Au core/shell nanospheres showed dramatically decreased electric field intensity in their proximity compared with the Ag nanospheres at their respective resonance wavelengths (Figure 1c). Therefore, isotropic Ag@Au core/shell nanocrystals demonstrated much poorer plasmonic properties than their Ag counterparts due to the coupling of the LSPR with the interband transitions. By clear contrast, the Ag@Au core/shell nanoplates showed an LSPR band with almost the same intensity as that of the Ag nanoplates (Figure 1b), suggesting that anisotropic Ag@Au nanostructures are able to support remarkable LSPR that is virtually Ag-like at wavelengths of >600 nm. The electric field near the Ag@Au core/shell nanoplates was weakened relative to that of the Ag nanoplates, which however is by far less significant (Figure 1d). Therefore, the plasmonic properties of the Ag@Au core/shell nanocrystals heavily rely on the shape anisotropy, with the anisotropic Ag@Au core/shell nanoplates possessing combined advantages of remarkable plasmonic properties and stability.

2.2. Synthesis, Plasmonic Properties, and Stability of the Ag@Au Core/Shell Nanoplates

The synthesis of Ag@Au core/shell nanocrystals, on the other hand, remains a great challenge. The key is to choose an appropriate ligand to the Au salt, which should satisfy the following requirements. First, the ligand should strongly coordinate to the Au salt to form a highly stable complex with significantly lowered reduction potential. As a consequence, Ag cannot compete with the additional reducing agent (typically ascorbic acid, AA) to undergo redox reactions with the Au complex, and thus galvanic replacement is reliably avoided. Second, because Ag nanocrystals are susceptible to oxidative etching assisted by many coordinating species,[19] the ligand of choice should avoid forming considerably strong complex with Ag^+ ions and thus is benign to the Ag nanocrystals in the mild reductive synthesis system. Many conventional ligands such as iodide (I^-) form highly stable complexes with both Au and Ag salts in mild reductive environments and thus are unsuitable for this synthesis. In our investigation, sulfite (SO_3^{2-}) was found to be an appropriate ligand to meet both requirements, which ensured continuous epitaxial growth of Au and thus successful conversion of Ag nanocrystals into Ag@Au core/shell counterparts.

First, the sulfite acts dually as a ligand and a reducing agent to produce a gold(I) sulfite complex, $Na_2Au(SO_3)_2$, which is already known as a gold plating agent.[20] This complex has particularly high stability ($pK_{sp} = -26.8$) and thus low reduction potential ($E^{\ominus} = 0.111$ V vs standard hydrogen electrode, SHE) under alkaline conditions.[20] For comparison, the reduction potentials of gold iodide complexes, AuI_4^- and AuI_2^-, which were used for atomic layer deposition of Au on Ag nanoplates in our previous study, are 0.56 and 0.58 V versus SHE, respectively.[4] Although all these values are well below the reduction potential of Ag^+ (0.8 V vs SHE) for favorable suppression of the galvanic replacement, the gold(I) sulfite complex with extremely decreased reduction potential makes complete suppression of the galvanic replacement possible during the epitaxial growth of Au on the Ag nanocrystals.

On the other hand, among different ligands, sulfite is one of the few choices that are benign to the Ag nanocrystals. To experimentally examine it, a solution containing polyvinylpyrrolidone (PVP), AA, NaOH, and Ag nanoplates was prepared for simulating the mild reductive environment of the synthesis, and different ligands such as Br^-, I^-, Cl^-, and SO_3^{2-} were added and analyzed by UV–vis spectroscopy (**Figure 2**). When exposed to Br^- or I^-, the Ag nanoplates underwent rapid spectral changes including a blueshift in the band position and a decrease in its intensity in the first few minutes, suggesting that the Ag nanoplates have been quickly destroyed by oxidative etching (Figure 2a,b). In clear contrast, no spectral changes have been observed in the presence of Cl^- and SO_3^{2-}, suggesting that the Ag nanoplates stayed intact (Figure 2c,d). The different etching behaviors can be attributed to the relatively weak coordination bonding of the Ag^+ with the ligands of Cl^- and SO_3^{2-}. It is worth noting that the solubility of the AgBr, AgI, AgCl, and Ag_2SO_3 complexes in terms of the Ag^+ concentration

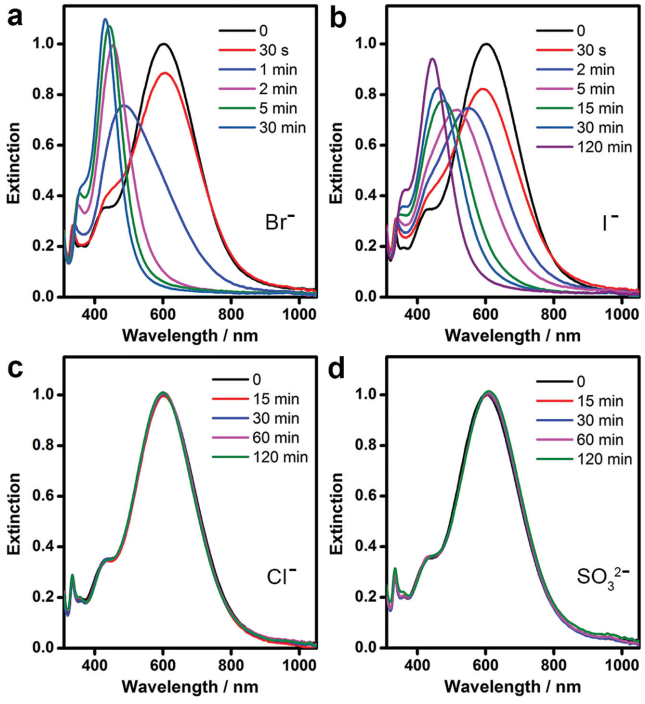

Figure 2. Etching effect of the ligands, a) Br^-, b) I^-, c) Cl^-, and d) SO_3^{2-}, on pristine Ag nanoplates. In a typical investigation, a mixture solution was prepared containing 500 µL of PVP (5 wt%), 100 µL of AA (0.5 M), 100 µL of NaOH (0.5 M), and 20 mL of the Ag nanoplates. To this solution was added 25 µL of the sodium salts of the ligands (0.1 M) prior to UV–vis spectroscopy measurement.

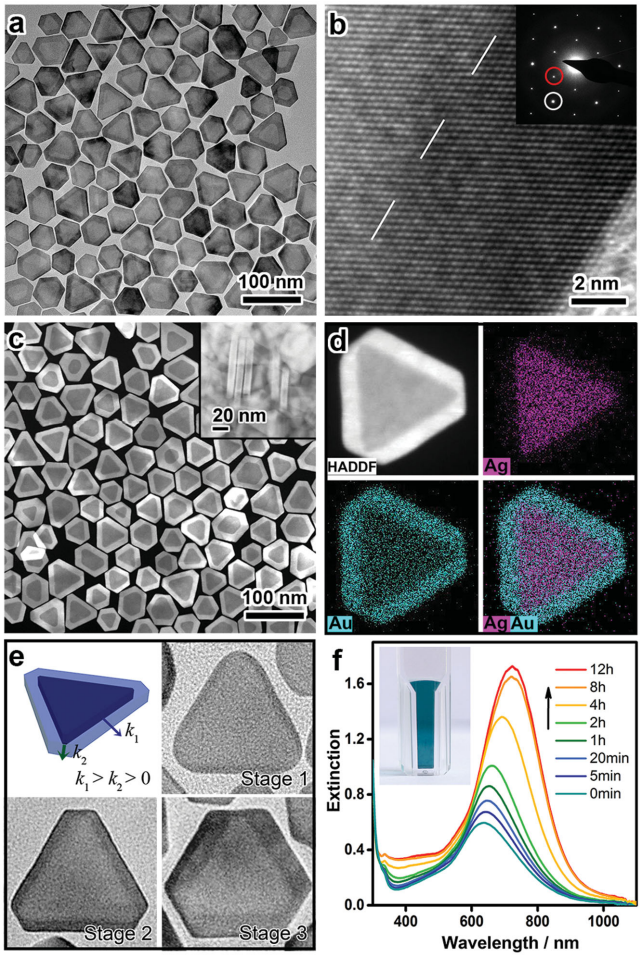

Figure 3. Synthesis of the truncated triangular Ag@Au core/shell nanoplates. a) TEM image of the nanoplates. b) HRTEM image. The dash line indicates approximate Ag/Au boundary judged from the image contrast (for full image see Figure S3, Supporting Information). Inset: Electron diffraction pattern. White and red circles indicate the {220} and formally forbidden 1/3{422} reflections, respectively. c) HAADF-STEM image of the nanoplates. d) EDS elemental mapping of an individual Ag@Au nanoplate. e) Growth intermediates of the Ag@Au nanoplates observed by TEM. The schematic cartoon illustrates the relative growth kinetics of Au on different sites of the Ag nanoplates. f) Evolution of the UV–vis extinction spectrum during the growth of the Ag@Au nanoplates. Inset: A digital photograph of a solution of the Ag@Au nanoplates.

in water can be calculated to be 0.73, 0.009, 13.3, and 31.1 × 10^{-3} M, respectively,[21] which suggests that the strength of the coordination bond with Ag^+ increases in the order of SO_3^{2-} < Cl^- < Br^- < I^-, consistent with our results. Between the ligands of Cl^- and SO_3^{2-} that are mild to the Ag nanocrystals, only SO_3^{2-} can form a highly stable complex with the Au salt, which enables continuous epitaxial growth of Au on the Ag nanocrystals without imposing any etching effect.

As a result, Ag@Au core/shell nanoplates (edge length: ≈55 nm; thickness: ≈9 nm) were readily obtained by the sulfite-aided epitaxial growth of Au on conventionally available Ag nanoplates (**Figure 3** and Figure S2, Supporting Information). The transmission electron microscopy (TEM) image (Figure 3a) indicates that uniform Ag@Au core/shell nanoplates were obtained in high yield. From the contrast of the image, it is clear that a uniform thick layer of Au with well-defined facets has been formed on the Ag nanoplates, and no voids can be observed suggesting the absence of galvanic replacement and ligand-assisted oxidative etching. High-resolution TEM (HRTEM) images of the sample (Figure 3b and Figure S3, Supporting Information) reveal that the Au layer was grown on the Ag nanoplates in a conformal epitaxial manner, with the single crystallinity and planar twins in the {111} direction retained indicated by the formally forbidden 1/3{422} reflections in the electron diffraction pattern.[14a] The Ag@Au core/shell structure of the Ag@Au nanoplates was further identified by high-angle annular dark-field scanning transmission electron microscopy (HAADF-STEM) and energy dispersive X-ray spectroscopy (EDS) elemental mapping (Figure 3c,d). The HADDF-STEM image of an individual nanoplate displays a gray triangular zone in the center enclosed by a much brighter zone on the edge, which can be attributed to the Ag core and the Au shell, respectively. EDS mapping reveals that the characteristic X-ray signals of Ag come exclusively from the core of the Ag@Au nanoplate, and the signals of Au come mainly from the edges. The edges of the Ag@Au nanoplates are thus composed of monometallic Au, with the reasons being twofold. First, the sulfite as a ligand prevents dissolution of the Ag nanoplates, so that coreduction of the Ag and Au salts has been avoided. Second, the epitaxial deposition of Au on Ag nanoplates finishes in a relatively short time at a low temperature, which suppresses the interfacial diffusion of the Ag and Au atoms. Therefore, unlike galvanic replacement that usually involves both processes to afford Ag/Au alloy nanocrystals,[15] the etching-free synthesis developed in this work gives rise to coating of monometallic Au on the Ag nanoplates.

It is worth noting that the rate of the epitaxial growth of Au on the Ag nanoplates exhibited site selectivity (Figure 3e). Growth intermediates of the Ag@Au core/shell nanoplates with increasing shell thickness were observed by TEM, which clearly showed growth of Au preferentially on the side facets of the Ag nanoplates over the corner facets. After a typical epitaxial growth, the thickness of the Au layer was measured to be ≈8 nm on the sides of the Ag nanoplates, but was only ≈2 nm at the corners and the basal facets. Sulfite thus served as the capping agent specifically to the {111} facets of the nanocrystals, which favored rapid growth of Au on the side facets of the Ag nanoplates that possess a large fraction of the {100} facets, while suppressed the growth of Au on the corner and basal facets that are usually composed of {111} facets.[22] As a result, the Ag@Au core/shell nanoplates were obtained as truncated triangular ones. Some other shapes of the Ag@Au core/shell nanoplates can be occasionally observed by TEM, which show significant growth of Au at their corners. It might be attributed to the different crystal structure of these individual nanoplates with a large fraction of {100} facets at the corners, as well as to the much extensive growth of the Au on these nanoplates.

The optical property of the Ag@Au core/shell nanoplates during the epitaxial growth was monitored by in situ UV–vis spectroscopy (Figure 3f). We observed a progressive redshift in the peak position and a continuous increase in the intensity. It confirms that galvanic replacement has been avoided in the synthesis, which otherwise is typically accompanied

by significant damping of the LSPR band due to the etching of the nanostructures.[15c] In addition, this spectral change is also distinct from those during the coating of Au on Ag nanoparticles with pseudoisotropic shapes such as spheres and cubes, which usually exhibit damped LSPR band due to the surface modification with Au of low extinction efficiency at their resonance wavelengths (an example discussed later).[16c] In our observation, the redshift of the LSPR band can be attributed to the increase in the aspect ratio of the Ag@Au nanoplates during the epitaxial growth, and the increasing intensity can be attributed dually to the effective separation of the LSPR band from the interband transitions and to the expanding volume of the nanoparticles.[23] The Ag@Au nanoplates thus showed outstanding plasmonic optical properties, which well validated our hypothesis that the plasmonic properties of the Ag@Au core/shell nanocrystals are anisotropy-dependent from an experimental perspective.

The sulfite-assisted etching-free epitaxial growth of Au can be applied to Ag nanospheres to afford Ag@Au core/shell nanospheres that represent typical isotropic plasmonic nanocrystals, making it possible to further examine the effect of the shape anisotropy on the plasmonic properties of the Ag@Au core/shell nanocrystals (**Figure 4**). Ag nanospheres were chosen as the seeds for the syntheses of both the pure Ag and Ag@Au core/shell nanospheres (Figure 4a). Because the seeded growth was conducted in a stoichiometric manner, the Ag and Ag@Au core/shell nanospheres can be obtained with the same size and concentration when equal amounts of the seeds and the precursor were used in the seeded synthesis (Figure 4b,c). The TEM images clearly showed an increased size of the nanospheres from ≈45 nm to ≈60 nm. During the seeded growth, the LSPR band of the Ag nanospheres shifted from 410 to 428 nm with significantly increased intensity (Figure 4d). However in the synthesis of the Ag@Au core/shell nanospheres, the LSPR band shifted to 505 nm of the wavelength that became virtually Au-like, with the intensity decreased relative to that of the original Ag nanospheres albeit the expanded volume of the nanocrystals. When the nanocrystals were obtained with the same size and concentration in water, the Ag@Au core/shell nanospheres showed much weaker LSPR band than the pure Ag nanospheres, which is in good agreement with the theoretical simulations (Figure 1a).

The Ag@Au core/shell nanocrystals displayed excellent stability against chemical etching in oxidative environments due to the presence of the thick layer of Au on their surfaces (**Figure 5**). The Ag@Au core/shell nanoplates were selected as an example, which showed negligible changes when exposed to hydrogen peroxide (H_2O_2) (Figure 5a and Figure S4, Supporting Information). The nanoplates even survived when exposed to much stronger oxidants such as $FeCl_3$ (0.5 M), showing only rounded corners, with corner Au atoms oxidized and etched away by the strongly oxidative Fe(III) ions (Figure 5b). However,

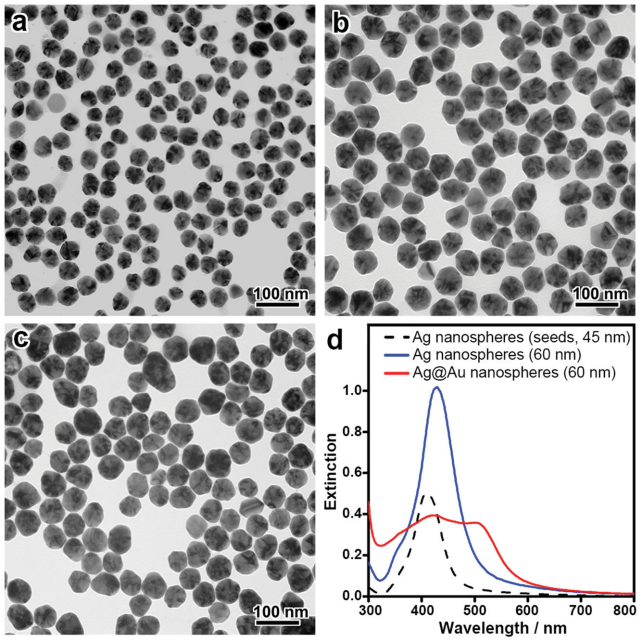

Figure 4. Synthesis and plasmonic property of the Ag@Au core/shell nanospheres in comparison with their Ag counterparts. a) TEM image of the Ag nanospheres (≈45 nm), which were the seeds for the synthesis of both the Ag and the Ag@Au core/shell nanospheres. b) TEM image of the Ag nanospheres (≈60 nm) after epitaxial growth of Ag on the Ag nanospheres. c) TEM image of the Ag@Au nanospheres (≈60 nm) after epitaxial growth of Au on the Ag nanospheres by the etching-free synthesis. The size and concentration of the Ag@Au nanospheres were the same as those of the Ag ones, which was ensured experimentally by deposition of the same amount of Au or Ag on a certain quantity of the Ag nanospheres (seeds). d) UV–vis spectra of the Ag seeds (≈45 nm), the Ag (≈60 nm), and Ag@Au nanospheres (≈60 nm) of the same concentration in water.

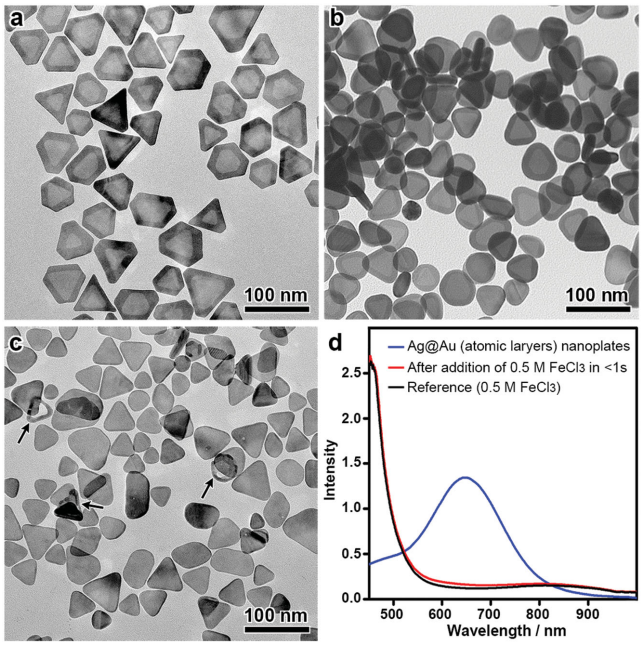

Figure 5. Chemical stability of the truncated triangular Ag@Au core/shell nanoplates with different thicknesses of the Au shells. a,b) TEM images of the Ag@Au nanoplates with a thick Au shell after treatment in a) H_2O_2 (1 M) for 48 h and in b) $FeCl_3$ (0.5 M) for 12 h, respectively. c) TEM image of the Ag@Au nanoplates with atomic layers of Au after treatment in H_2O_2 (1 M) for 48 h. Arrows indicate nanoplates that are less stable in the oxidative environment. d) UV–vis spectra of the Ag@Au nanoplates with atomic layers of Au upon mixing with a strongly oxidative solution of 0.5 M $FeCl_3$.

no hollowing or deformation of the core/shell nanostructure has been observed, which confirmed the high stability of the Ag@Au core/shell nanoplates. For comparison, Ag nanoplates with a thin layer of Au were stable in H_2O_2 with occasionally observed destabilized nanoplates (Figure 5c), but were completely destroyed upon exposure to $FeCl_3$ (0.5 M) as evidenced by the fully disappeared LSPR band in the UV–vis spectrum (Figure 5d). Therefore, the thick Au layer is essential for the Ag@Au core/shell nanoplates to display excellent stability in strongly oxidative environments. The Ag@Au core/shell nanoplates with a thick layer of Au are thus a combination of excellent plasmonic properties and high stability, which makes them particularly useful in many plasmon-based applications for enhanced performance and duration in the presence of interfering chemicals.

2.3. Synthesis of Ag@Au Core/Shell Nanoplates with Tunable Size, Structures, and Plasmonic Properties

Due to the robust mechanism in effectively suppressing both the destructive galvanic replacement and the oxidative etching, this synthesis is highly adaptable to yield truncated triangular Ag@Au nanoplates of different sizes and morphologies for extended plasmonic properties in a wide range of the spectrum. As a demonstration, Ag nanoplates of different sizes were chosen as the seeds, and truncated triangular Ag@Au nanoplates were successfully synthesized by following a similar procedure as described above (**Figure 6**). The TEM images of the samples clearly showed epitaxial growth of Au on the Ag nanoplates indicated by the image contrast of the cores and the edges of the nanoplates. Their in-plane dipole LSPR bands were located in a wide range of the spectrum ranging from 720 nm (edge length of the nanoplates: ≈55 nm) to 1090 nm (edge length of the nanoplates: ≈232 nm) of the wavelength, which well covered the tissue optical window that is important for many biological applications. Well-defined quadrupole mode LSPR bands can be observed in the UV–vis–NIR spectra, suggesting that the large Ag@Au core/shell nanoplates are highly uniform in size and morphology. This synthesis approach may provide further opportunities in the synthesis of Ag@Au core/shell nanoplates with much greater tunability in size and plasmonic property for a broad range of applications such as fabrication of optical and electronic nanodevices.

In another demonstration, starting from the Ag nanoplates, hexagonal Ag@Au core/shell nanoplates can be obtained instead of truncated triangular ones by tuning the reaction kinetics of the epitaxial growth (**Figure 7**). The TEM (Figure 7a) revealed the high yield production of the hexagonal Ag@Au core/shell nanoplates, with the Ag core and the Au shell identified by HAADF-STEM (Figure S6, Supporting Information) and the EDS elemental mapping (Figure 7a, inset). The nanoplates were measured to be ≈15 nm in thickness from the vertically aligned ones on the TEM grid. The hexagonal Ag@Au nanoplates are single crystals with twin planes confirmed by HRTEM and the electron diffraction pattern (Figure 7b and Figure S7, Supporting Information). The key of the synthesis was to introduce acetonitrile as an additional ligand to the Au cations (Figure S5, Supporting Information), which further

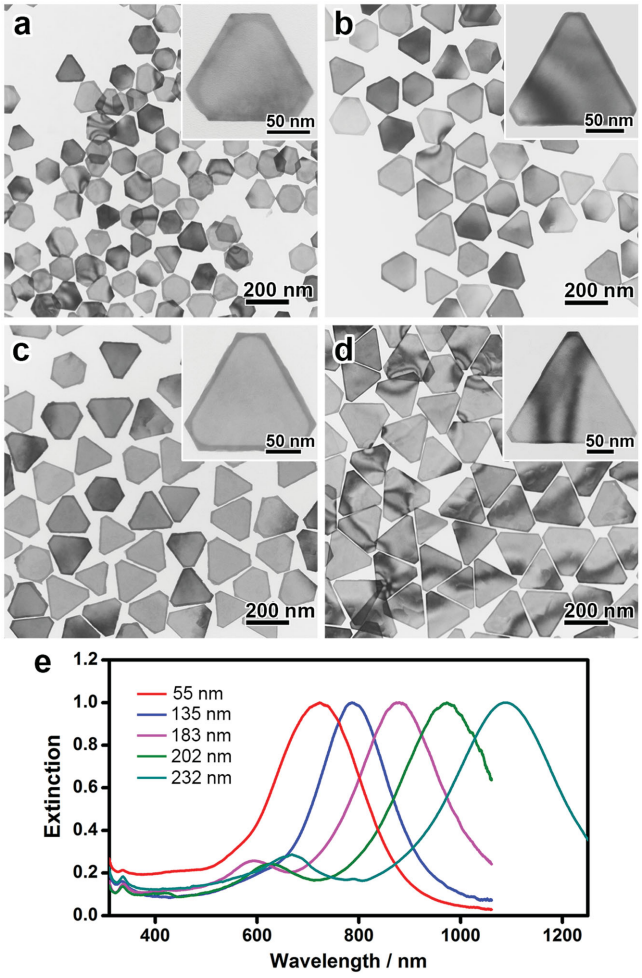

Figure 6. Synthesis of truncated triangular Ag@Au core/shell nanoplates with varying sizes. a–d) TEM images of the Ag@Au nanoplates with average edge lengths of 135, 183, 202, and 232 nm, respectively. e) UV–vis–NIR spectra of the Ag@Au nanoplates dispersed in H_2O.

reduced the reaction rate as evidenced by the much-decelerated change in the UV–vis spectroscopy (Figure 7c). As a result, the growth of Au exhibited greater site selectivity, with the growth largely blocked on the corners of the triangular nanoplates (Figure 7d). The significant difference in the deposition rates of Au at the corners and the sides of the Ag nanoplates led to quick diminishing of the side facets and thus hexagonal morphology of the Ag@Au core/shell nanoplates (Figure 7d, Stages 1 and 2). Extended epitaxial growth of the Au gave rise to much thicker nanocrystals that became virtually isotropic nanospheres after 180 h of the growth (Figure 7d, Stage 3). As a result, the LSPR band shifted continuously from 615 to 515 nm owing to the shape transformation of the triangular nanoplates into hexagonal ones as well as the increasing thickness (Figure 7c). The intensity, however, rose initially and then dropped, albeit the continuously expanded volume of the nanoplates that theoretically leads to progressively enhanced extinction efficiency. This unusual observation can be attributed to the coupling of the LSPR with interband transitions of Au at short wavelengths of the spectrum. It therefore again validated our hypothesis that

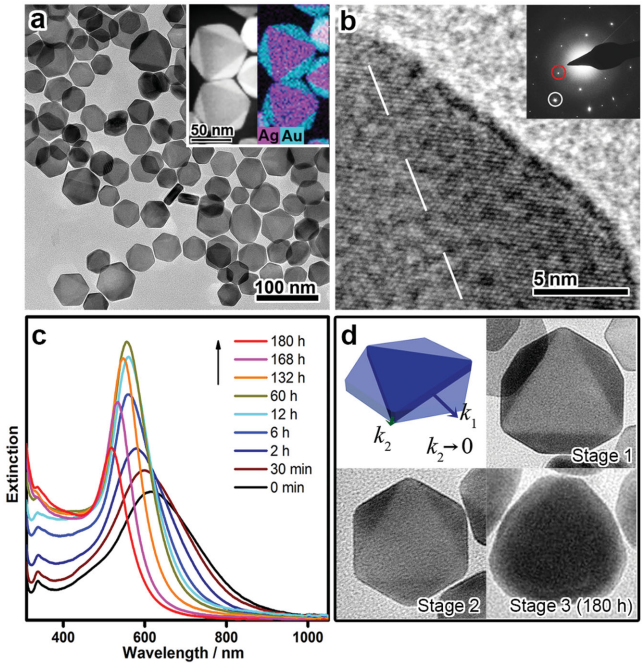

Figure 7. Synthesis of hexagonal Ag@Au core/shell nanoplates. a) TEM image of the nanoplates. Inset: Elemental mapping of an individual nanoplate. b) HRTEM image. The dash line indicates approximate Ag/Au boundary judged from the contrast of the image (for full image see Figure S7, Supporting Information). Inset: Electron diffraction pattern. White and red circles indicate the {220} reflection and the formally forbidden 1/3{422} reflection, respectively. c) Evolution of the UV–vis extinction spectroscopy during the growth of the hexagonal Ag@Au nanoplates. d) Growth intermediates of the hexagonal Ag@Au nanoplates observed by TEM. The schematic cartoon illustrates the growth kinetics of Au on different sites of the Ag nanoplates.

the high anisotropy of the Ag@Au nanocrystals is essential for them to support optimal optical properties for plasmonic applications.

2.4. Plasmon-Based Applications of the Ag@Au Core/Shell Nanoplates

The remarkable stability and the Ag-like plasmonic properties of the anisotropic Ag@Au nanoplates enable their wide use particularly in plasmon-based applications where interfering oxidative species are involved. As a demonstration, SERS detection of crystal violet (CV) was conducted in the presence of Fe^{3+} or H_2O_2, which represents common oxidative impurities in practical analyses (**Figure 8**). In a typical measurement, Ag and Ag@Au nanoplates of the same concentration and volume were added into aqueous solutions of CV containing an intentionally added oxidative impurity, which were subjected to SERS analysis using 633 nm excitation (Figure 8a,b). We collected SERS spectra from aqueous solutions because the LSPR bands of the Ag and the Ag@Au nanoplates are both close to the excitation wavelength when they are dispersed in water. Our results showed that both nanoplates exhibited high activities in detecting CV in the absence of any oxidative impurity, and well-resolved Raman signals of comparable intensity were observed at 1177, 1378, and 1615 cm^{-1} of the Raman shift which are typical of the CV molecules. The signals from the Ag@Au nanoplates were slightly lower, which can be attributed to the lower electric field intensity in their proximity and the deviation of excitation wavelength from the resonance wavelength of the nanoplates in the analysis. When 2 M Fe^{3+} or H_2O_2 was present in the analyte solution, the SERS signals from the Ag nanoplates were drastically decreased, suggesting that the Ag nanoplates were destroyed by the oxidative impurities. By contrast, no obvious effects of the impurities can be found on the intensity of the SERS signals from the Ag@Au ones. Therefore, the Ag@Au nanoplates developed in this work are superior in reliable SERS detection of target molecules in an unknown solution which may have a complex composition. It is worth noting that the detection limit of CV can be further reduced to $\approx 10^{-8}$ M in our experiment for even sensitive analysis by depositing the Ag@Au nanoplates on silicon substrates (Figure 8c).

3. Conclusion

In summary, we have demonstrated a robust epitaxial deposition method for the synthesis of anisotropic Ag@Au nanostructures which showed combined advantages of excellent chemical stability and plasmonic properties. Sulfite played a critical role in enabling the continuous epitaxial growth of Au on the Ag nanocrystals because it strongly coordinates to the gold precursor but is mild to the Ag nanocrystals in the synthesis, which favors suppression of both galvanic replacement and oxidative etching of the Ag nanocrystals, and thus enables continuous epitaxial growth of Au on the Ag nanocrystals. As a specific example, Ag@Au nanoplates developed in this work showed high stability and remarkable optical properties which are virtually Ag-like. These Ag@Au nanoplates are thus particularly useful in many plasmon-based applications where interfering species are usually involved. As a demonstration, these Ag@Au nanoplates showed superior performance against Ag nanoplates in SERS detection of molecules of interest in the presence of Fe^{3+} and H_2O_2. It is believed that this synthesis method is general and extendable to the coating of a noble metal, such as Au and Pt, on a diversity of less stable metal substrates such as spheres, cubes, plates, rods, and wires of Ag or Cu, thus opening up new opportunities in the rational design of metal nanomaterials for many optical, electronic, biological, analytical, and catalytic applications.

4. Experimental Section

Synthesis of Ag Nanoplates (Seeds): Silver nanoplates were synthesized according to the procedure reported by Mirkin and co-worker with minor modifications.[14b] Typically, 0.2 mL of $AgNO_3$ (0.1 M), 12 mL of trisodium citrate (0.075 M), and 0.48 mL of H_2O_2 (30 wt%) were dissolved in 200 mL of H_2O. Then, 1.2 mL of $NaBH_4$ (0.1 M) was quickly injected into the solution under vigorous stirring. After 30 min, the resulting solution was used as the stock solution of Ag nanoplates without further purification.

Preparation of Growth Solution of Au: In 4.72 mL of H_2O were added in sequence 40 μL of $HAuCl_4$ (0.25 M), 240 μL of NaOH (0.2 M), and

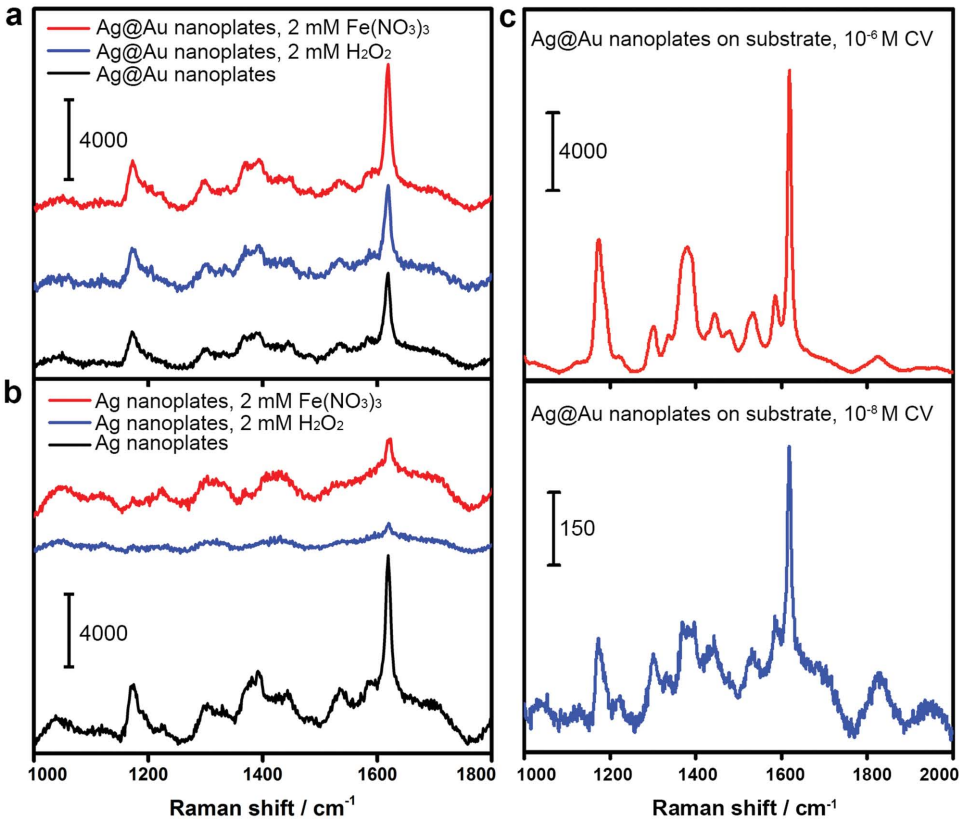

Figure 8. a,b) SERS spectra recorded from aqueous solutions of crystal violet (CV, 10^{-5} M) enhanced by the Ag@Au and Ag nanoplates, respectively, in the presence of impurity reagents including 2×10^{-3} M Fe^{3+} and H_2O_2. c) SERS spectra of CV with concentrations as low as 10^{-6} M and 10^{-8} M recorded from a silicon substrate deposited with the Ag@Au nanoplates.

3.00 mL of Na_2SO_3 (0.01 M). The solution was left undisturbed overnight before use.

Synthesis of Truncated Triangular Ag@Au Core/Shell Nanoplates: In a typical synthesis, Ag nanoplates were centrifuged from 40 mL of their stock solution and redispersed in 2 mL of H_2O. A solution was prepared by mixing 2.55 mL of H_2O, 1 mL of PVP (5 wt%, M_w 40 000), 200 µL of L-AA (0.5 M), 200 µL of NaOH (0.5 M), 50 µL of Na_2SO_3 (0.1 M), and 4 mL of the growth solution of Au in a glass vial, which was then merged with the solution of the Ag nanoplates to initiate the seeded growth. The reaction was then allowed to proceed undisturbed at 30 °C for 12 h. Finally, Ag@Au nanoplates were collected by centrifugation and washed with H_2O. It is worth noting that the reaction time can be significantly shortened to 1 h by increasing the reaction temperature to 60 °C, which facilitates rapid synthesis of Ag@Au nanoplates for mass production (Figure S8, Supporting Information).

Synthesis of Truncated Triangular Ag@Au Core/Shell Nanoplates with Varying Sizes: To achieve the size tuning of the truncated triangular Ag@Au core/shell nanoplates, Ag nanoplates of different sizes were synthesized by our earlier reported seeded growth method,[14d] which were then used as the seeds for the epitaxial growth of Au following a similar procedure as described above.

Synthesis of Hexagonal Ag@Au Core/Shell Nanoplates: In a typical synthesis, Ag nanoplates were centrifuged from 40 mL of their stock solution and redispersed in 2 mL of H_2O. A solution was prepared by mixing 1.6 mL of H_2O, 1 mL of CH_3CN, 1 mL of PVP (5 wt%), 200 µL of AA (0.5 M), 200 µL of NaOH (0.5 M), and 4 mL of the growth solution of Au in a glass vial, which was then merged with the solution of the Ag nanoplates to initiate the seeded growth. The reaction was kept undisturbed at 25 °C for 12 h. Hexagonal Ag@Au nanoplates were then collected by centrifugation and washed with H_2O.

FEM Simulation: The 3D FEM simulation was used to calculate extinction spectra and electric field distributions of the plasmonic nanostructures under laser excitation. The incident laser was in the form of a plane wave, which propagated along the *z*-axis and polarized along the *x*-axis. It was assumed that each geometrical model was suspended in water. To avoid nonphysical reflections of outgoing electromagnetic waves from the grid boundaries, perfectly matched layers of absorbing boundaries were employed around the targets.

Surface-Enhanced Raman Spectroscopy: Ag and Ag@Au nanoplates of the same concentration and volume were incubated with an aqueous solution containing 10^{-5} M crystal violet (CV) and 2×10^{-3} M $Fe(NO_3)_3$ or H_2O_2 for 2 h. Raman spectra were then recorded from the suspension with a 633 nm He-Ne laser line at room temperature. For all measurements, power density of the laser irradiation was 3 mW cm^{-2}, and the signal acquisition time was fixed to be 20 s. In a typical SERS analysis of CV on silicon substrate, 25 µL of the Ag@Au nanoplates and 25 µL of CV (10^{-6} or 10^{-8} M) were dried on a silicon substrate in vacuum in sequence. The substrate was washed, dried in vacuum, and subjected to SERS analysis with a 633 nm He-Ne laser line. Laser spots were 0.85 µm under a 100× objective, power density was 0.3 mW cm^{-2}, and the signal acquisition time was 10 s.

Characterizations: HRTEM and HAADF-STEM were performed with an FEI Tecnai F20 FEG-TEM microscope operating at 200 kV. UV–vis spectra were measured on an Ocean Optics HR2000+ES spectrophotometer. UV–vis–NIR spectra were measured on a Shimadzu UV-3600 UV–vis–NIR spectrophotometer. Raman spectra were collected using a LabRAM HR800 confocal Raman spectrophotometer equipped with 633 nm He-Ne laser.

Supporting Information

Supporting Information is available from the Wiley Online Library or from the author.

Acknowledgements

C.G. acknowledges support from the National Natural Science Foundation of China (Grant No. 21301138), the startup fund, and operational fund for the Center for Materials Chemistry from Xi'an Jiaotong University. Y.Y. acknowledges support from the U.S. National Science Foundation (CHE-1308587). L.H. acknowledges support from the National Natural Science Foundation of China (Grant No. 21201120).

Received: June 10, 2015
Revised: July 6, 2015
Published online: August 6, 2015

[1] a) M. Rycenga, C. M. Cobley, J. Zeng, W. Li, C. H. Moran, Q. Zhang, D. Qin, Y. Xia, *Chem. Rev.* **2011**, *111*, 3669; b) K. A. Willets, R. P. Van Duyne, *Annu. Rev. Phys. Chem.* **2007**, *58*, 267.

[2] a) M. J. Mulvihill, X. Y. Ling, J. Henzie, P. Yang, *J. Am. Chem. Soc.* **2009**, *132*, 268; b) Y. C. Cao, R. Jin, C. A. Mirkin, *Science* **2002**, *297*, 1536; c) S. Nie, S. R. Emory, *Science* **1997**, *275*, 1102; d) S. Schlücker, *Angew. Chem. Int. Ed.* **2014**, *53*, 4756; e) C. Gao, Y. Hu, M. Wang, M. Chi, Y. Yin, *J. Am. Chem. Soc.* **2014**, *136*, 7474.

[3] a) N. S. Abadeer, M. R. Brennan, W. L. Wilson, C. J. Murphy, *ACS Nano* **2014**, *8*, 8392; b) C. Ayala-Orozco, J. G. Liu, M. W. Knight, Y. Wang, J. K. Day, P. Nordlander, N. J. Halas, *Nano Lett.* **2014**, *14*, 2926.

[4] C. Gao, Z. Lu, Y. Liu, Q. Zhang, M. Chi, Q. Cheng, Y. Yin, *Angew. Chem. Int. Ed.* **2012**, *51*, 5629.

[5] K. A. Homan, M. Souza, R. Truby, G. P. Luke, C. Green, E. Vreeland, S. Emelianov, *ACS Nano* **2011**, *6*, 641.

[6] S. Lal, S. E. Clare, N. J. Halas, *Acc. Chem. Res.* **2008**, *41*, 1842.

[7] a) P. Christopher, H. Xin, S. Linic, *Nat. Chem.* **2011**, *3*, 467; b) M. Murdoch, G. I. N. Waterhouse, M. A. Nadeem, J. B. Metson, M. A. Keane, R. F. Howe, J. Llorca, H. Idriss, *Nat. Chem.* **2011**, *3*, 489; c) F. Wang, C. Li, H. Chen, R. Jiang, L.-D. Sun, Q. Li, J. Wang, J. C. Yu, C.-H. Yan, *J. Am. Chem. Soc.* **2013**, *135*, 5588; d) R. Jiang, B. Li, C. Fang, J. Wang, *Adv. Mater.* **2014**, *26*, 5274.

[8] M.-C. Daniel, D. Astruc, *Chem. Rev.* **2003**, *104*, 293.

[9] H. Wang, F. Tam, N. K. Grady, N. J. Halas, *J. Phys. Chem. B* **2005**, *109*, 18218.

[10] a) N. R. Jana, L. Gearheart, C. J. Murphy, *Adv. Mater.* **2001**, *13*, 1389; b) B. Nikoobakht, M. A. El-Sayed, *Chem. Mater.* **2003**, *15*, 1957; c) X. Ye, Y. Gao, J. Chen, D. C. Reifsnyder, C. Zheng, C. B. Murray, *Nano Lett.* **2013**, *13*, 2163.

[11] a) L. Chen, F. Ji, Y. Xu, L. He, Y. Mi, F. Bao, B. Sun, X. Zhang, Q. Zhang, *Nano Lett.* **2014**, *14*, 7201; b) J. E. Millstone, S. Park, K. L. Shuford, L. Qin, G. C. Schatz, C. A. Mirkin, *J. Am. Chem. Soc.* **2005**, *127*, 5312.

[12] R. Weissleder, *Nat. Biotechnol.* **2001**, *19*, 316.

[13] X. Lu, M. Rycenga, S. E. Skrabalak, B. Wiley, Y. Xia, *Annu. Rev. Phys. Chem.* **2009**, *60*, 167.

[14] a) R. Jin, Y. Cao, C. A. Mirkin, K. L. Kelly, G. C. Schatz, J. G. Zheng, *Science* **2001**, *294*, 1901; b) G. S. Métraux, C. A. Mirkin, *Adv. Mater.* **2005**, *17*, 412; c) J. E. Millstone, S. J. Hurst, G. S. Metraux, J. I. Cutler, C. A. Mirkin, *Small* **2009**, *5*, 646; d) Q. Zhang, Y. Hu, S. Guo, J. Goebl, Y. Yin, *Nano Lett.* **2010**, *10*, 5037; e) J. Zeng, X. Xia, M. Rycenga, P. Henneghan, Q. Li, Y. Xia, *Angew. Chem. Int. Ed.* **2011**, *50*, 244; f) Q. Zhang, N. Li, J. Goebl, Z. Lu, Y. Yin, *J. Am. Chem. Soc.* **2011**, *133*, 18931; g) X. Liu, L. Li, Y. Yang, Y. Yin, C. Gao, *Nanoscale* **2014**, *6*, 4513.

[15] a) Y. Sun, B. T. Mayers, Y. Xia, *Nano Lett.* **2002**, *2*, 481; b) X. Xia, Y. Wang, A. Ruditskiy, Y. Xia, *Adv. Mater.* **2013**, *25*, 6313; c) G. S. Métraux, Y. C. Cao, R. Jin, C. A. Mirkin, *Nano Lett.* **2003**, *3*, 519.

[16] a) M. M. Shahjamali, M. Bosman, S. Cao, X. Huang, S. Saadat, E. Martinsson, D. Aili, Y. Y. Tay, B. Liedberg, S. C. J. Loo, H. Zhang, F. Boey, C. Xue, *Adv. Funct. Mater.* **2012**, *22*, 849; b) N. Murshid, I. Gourevich, N. Coombs, V. Kitaev, *Chem. Commun.* **2013**, *49*, 11355; c) Y. Yang, J. Liu, Z.-W. Fu, D. Qin, *J. Am. Chem. Soc.* **2014**, *136*, 8153.

[17] C. Gao, J. Goebl, Y. Yin, *J. Mater. Chem. C* **2013**, *1*, 3898.

[18] J.-M. Jin, J. L. Volakis, J. D. Collins, *IEEE Antennas Propag. Mag.* **1991**, *33*, 22.

[19] a) B. Wiley, T. Herricks, Y. Sun, Y. Xia, *Nano Lett.* **2004**, *4*, 1733; b) J. An, B. Tang, X. Zheng, J. Zhou, F. Dong, S. Xu, Y. Wang, B. Zhao, W. Xu, *J. Phys. Chem. C* **2008**, *112*, 15176.

[20] T. A. Green, *Gold Bull.* **2007**, *40*, 105.

[21] J. A. Dean, *Lange's Handbook of Chemistry*, McGraw-Hill, New York, NY **1972**.

[22] a) D. Aherne, D. M. Ledwith, M. Gara, J. M. Kelly, *Adv. Funct. Mater.* **2008**, *18*, 2005; b) J. Goebl, Q. Zhang, L. He, Y. Yin, *Angew. Chem. Int. Ed.* **2012**, *51*, 552.

[23] S. Link, M. A. El-Sayed, *J. Phys. Chem. B* **1999**, *103*, 8410.